Erasing odd-parity states in semiconductor quantum dots coupled to superconductors

Z. Su,[1] R. Žitko,[2] P. Zhang,[1] H. Wu,[1] D. Car,[3] S. R. Plissard,[4] S. Gazibegovic,[3] G. Badawy,[3] M. Hocevar,[5] J. Chen,[1,6] E. P. A. M. Bakkers,[3] and S. M. Frolov[1]

[1]*Department of Physics and Astronomy, University of Pittsburgh, Pittsburgh, Pennsylvania 15260, USA*

[2]*Jožef Stefan Institute, Jamova 39, Ljubljana, Slovenia and Faculty of Mathematics and Physics, University of Ljubljana, Jadranska 19, Ljubljana, Slovenia*

[3]*Eindhoven University of Technology, 5600 MB, Eindhoven, Netherlands*

[4]*LAAS CNRS, Université de Toulouse, 31031 Toulouse, France*

[5]*Universite Grenoble Alpes, CNRS, Grenoble INP, Institut Néel, 38000 Grenoble, France*

[6]*Department of Electrical and Computer Engineering, University of Pittsburgh, Pittsburgh, Pennsylvania 15261, USA*

(Received 10 April 2019; accepted 26 May 2020; published 22 June 2020)

Quantum dots are gate-defined within InSb nanowires, in proximity to NbTiN superconducting contacts. As the coupling between the dot and the superconductor is increased, the odd-parity occupation regions in transport become nondiscernible (erased) both above and below the induced superconducting gap. Above the gap, conductance in the odd Coulomb-blockade valleys increases until the valleys are lifted. Below the gap, Andreev bound states undergo quantum phase transitions to Kondo-screened singlet ground states at odd occupancy. We investigate to what degree the apparent erasure of odd-parity regimes coincides at low and high biases. We complement experiments with numerical renormalization group simulations. We interpret the results in terms of a competition between Kondo screening and superconductivity. In the erased odd-parity regime, the quantum dot exhibits transport features similar to a finite-size Majorana nanowire, drawing parallels between even-odd dot occupations and even-odd one-dimensional subband occupations.

DOI: 10.1103/PhysRevB.101.235315

The prospect of topological quantum computing has motivated recent studies of charge parity, which is an observable that can distinguish the states of a Majorana quantum bit [1]. Experiments have demonstrated that electrons can be added to small superconducting islands either in pairs or one at a time, depending on the interplay of energy scales of the system [2–5]. Quantum jumps of parity have been observed in superconducting circuits [6,7]. In quantum dots coupled to superconductors, a quantum phase transition (QPT) between odd- and even-parity ground states has been investigated theoretically [8–14] and experimentally [15–27].

In this paper, we study the transition from the closed to the open regime (i.e., weak hybridization to strong hybridization regime) in a quantum dot defined in a semiconductor nanowire with superconducting contacts. We demonstrate how the transport signatures of odd-parity quantum-dot states are erased in the open dot regime. At source-drain biases that exceed the induced superconducting gap, we observe a transition from well-defined Coulomb diamonds to a conductance modulation pattern in which odd-occupancy Coulomb-blockade valleys rise in conductance faster than even valleys do. At low biases below the gap, we concurrently observe Andreev bound states (ABSs) that cross zero energy at every change in ground state parity from even to odd, while in the open regime the ABSs do not cross zero bias. This is a manifestation of the above-mentioned QPT. The experimental observations pose a question: Are phenomena observed at low and at high biases related or simply coincident?

In an attempt to answer this question, we make use of the numerical renormalization group (NRG) to perform theoretical simulations of the Anderson impurity model in a wide range of parameters beyond those accessible in the experiment. Our intuition is that Kondo physics is relevant as it can affect transport both at zero and at finite bias voltages. We find that if the high-bias range is defined to be of the order of the gap Δ (i.e., a few times Δ), the ABS QPT at low bias indeed coincides with the lifting of the odd Coulomb valleys at high bias. If the high-bias range is defined to be of the order of Coulomb energy (i.e., a significant fraction of the electron-electron repulsion parameter U), the correspondence is less clear-cut, because the relevant scale smoothly evolves from the Kondo temperature to the bare hybridization strength Γ as the bias voltage is increased. Nevertheless, the crossover points remain close by for experimentally relevant parameter sets.

In the same system, we furthermore find similarities between the evolution of ABS and the emergence of Majorana bound states (MBSs). Specifically, the phase diagram of the ABS QPT in gate voltage and magnetic field is reminiscent of the phase diagram predicted for the topological superconducting phase, if even-odd dot occupations are replaced with even-odd subband occupations. This highlights the persistent need to identify truly unique signatures of MBSs and to deeper study the related regime of trivial ABSs.

InSb nanowires are grown using metalorganic vapor phase epitaxy and transferred onto metallic gate patterns which are lines with 60–80 nm center-to-center pitch. The gates are covered by 10 nm of HfO_2 dielectric. NbTiN superconducting contacts are fabricated on top of the nanowire. The device in Fig. 1(a) is highly tunable: Previous reports on the same

 ©2020 American Physical Society

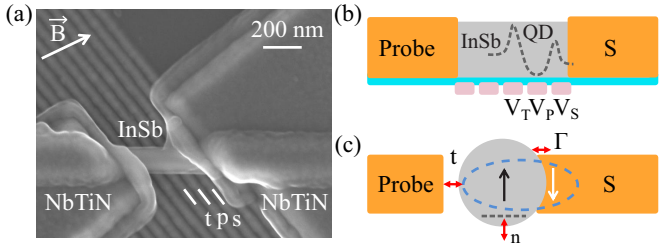

FIG. 1. (a) Scanning electron micrograph of the device studied in the main text: InSb nanowire in contact with superconducting NbTiN contacts. The arrow indicates the direction of the applied magnetic field, gates t, p, s are labeled. (b) Side-view schematic of the device: Superconducting contacts (orange), nanowire (grey), gate electrodes (pink), dielectric (blue), dashed line is an approximate potential created by gates to form a quantum dot (QD). (c) Superconductor on the right couples to the dot with hybridization Γ, while the superconductor on the left acts as a probe (hybridization t).

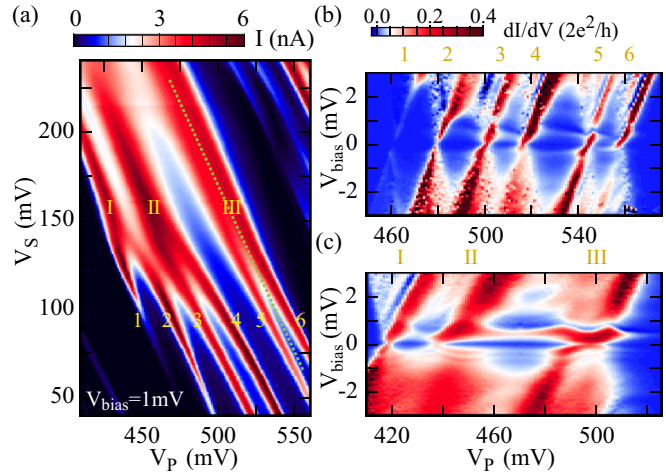

FIG. 2. (a) Current across the device at bias voltage $V_{bias} = 1$ mV versus gate voltages V_P and V_S. The arabic numerals $1-6$ denote the Coulomb peaks in the weak-coupling regime, the latin numerals I, II, III indicate the broad resonances in the strong-coupling regime. Current along the dashed green-line plotted in Fig. 3(g). (b) Finite-bias spectroscopy at weak coupling ($V_S = 75$ mV) shows six Coulomb diamonds and in-gap states forming loops at low bias, $V_{bias} \lesssim 0.4$ mV. (c) Finite-bias spectroscopy at strong coupling ($V_S = 150$ mV) shows broad ($2e$) resonances at high bias and anticrossing subgap features at low bias. $V_T = -555$ mV.

device demonstrated that it can be used to set up a quantum dot near the left or the right superconductor, as well as a double dot [28,29]. Here a single quantum dot is defined using gates t, p, s near the right superconductor. The left barrier is primarily controlled by gate t which is fixed near pinch-off, $V_T = -555$ mV, so tunneling to the left is much weaker than tunneling to the right. The barrier controlled by the voltage V_S on gate s tunes Γ, the coupling to the right superconductor [Fig. 1(b)]. The voltage on gate p, V_P primarily controls the dot chemical potential μ or the number of electrons n. The minimal two-terminal resistance of the device is 4 kΩ. Measurements are performed in a dilution refrigerator with a base temperature of 40 mK.

The key experimental observations of the paper are presented in Figs. 2 and 3. For $V_S < 100$ mV, the quantum dot is in the Coulomb blockade regime. We observe a sequence of Coulomb peaks by tuning V_P; we label these peaks 1 through 6 in Figs. 2(a) and 2(b). For $V_S > 100$ mV and with increasing V_S, Coulomb peaks are continuously merging pairwise into broad resonances labeled I, II, III in Figs. 2(a) and 2(c). Figure 2(a) is obtained under a source drain bias voltage $V_{bias} = 1$ mV which is somewhat above the apparent induced gap, but below the bulk gap of NbTiN. The current in every other Coulomb valley increases with higher V_S, i.e., the odd valleys are being lifted.

The effect of transitioning from $1e$ to $2e$ conductance pattern in nonsuperconducting open quantum dots, or in dots coupled to gapless (soft gap) superconductors, can be qualitatively understood in terms of Kondo physics (for $U/\Gamma > \pi$) or in terms of charge-quantization loss (for $U/\Gamma < \pi$); the evolution between these two regimes is a smooth crossover. The erasure is thus in principle a two-step process but the second step is not necessarily clearly discernible. Starting from the deep Coulomb-blockade regime with $U/\Gamma \gg \pi$ and negligible Kondo temperature, $T_K \ll T, V_{bias}$, by making the barrier more transparent with increasing hybridization strength Γ, the Kondo temperature T_K increases and eventually exceeds the scale of T and V_{bias}. When this happens, the conductance in odd-occupancy Coulomb-blockade valleys increases and gives rise to Kondo plateaux. The quantum dot occupancy is still quantized in this regime. As Γ increases further, the local moment is lost at $U/\Gamma \approx \pi$ and the occupancy in the dot no longer varies in steps of 1, hence the Kondo plateaux are replaced by trivial conductance peaks with width dictated by Γ [30].

At lower biases, a set of horizontal resonances near $V_{bias} = 0.4$ mV is observed [Figs. 2(b) and 2(c)]. In Fig. 2(b), the horizontal resonances appear to coexist with Coulomb resonances 1–6. Such resonances have been reported in quantum dots with superconducting contacts and are either related to cotunneling enhanced by high density of states at the gap edge [18] or related to ABSs in the dot. In Fig. 2(c), at higher V_S, when the coupling to the right superconductor is increased, the horizontal resonances are still present, but the Coulomb peaks are absent. Instead, the zero-bias conductance exhibits a local minimum throughout the range of V_P. At high bias, Coulomb diamonds are replaced with three broader resonances I, II, III.

The detailed evolution of low-bias superconductivity-related resonances as a function of V_S is shown in Figs. 3(a)–3(f), which is focusing on the region labeled III in Fig. 2. For low V_S [Figs. 3(a)– 3(b)], the resonances form a loop around zero bias. The loop shrinks with increasing V_S until the two zero-bias crossings merge around $V_S = 100$ mV [Fig. 3(c)]. For higher V_S, the horizontal resonances at positive and negative biases exhibit an anticrossing, its level repulsion growing with more positive V_S [Figs. 3(d)– 3(f)]. The Supplemental Material contains comprehensive data on the evolution from the closed to open dot regime over wider ranges of V_{bias} and V_P [31].

This transition from looplike to anticrossinglike resonances has been previously studied as a manifestation of the

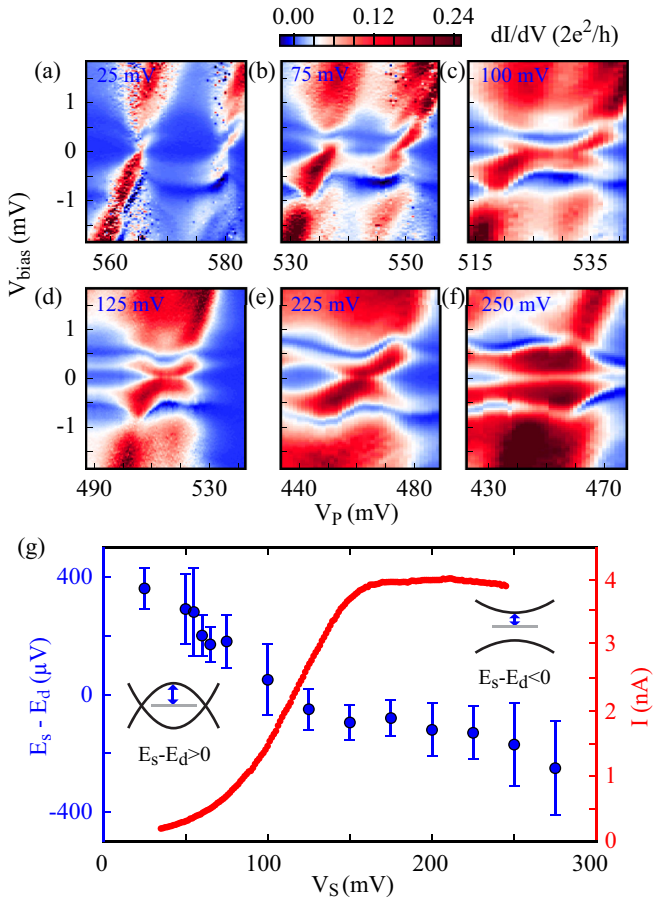

FIG. 3. (a)–(f) Evolution of the finite-bias spectra of the odd Coulomb valley III from weak to strong coupling. The gate voltage V_S is indicated in blue in the upper left of each panel. (g) Comparison of the singlet-doublet energy difference (blue points) and the finite-bias current in valley III (red line).

singlet-doubled QPT at odd quantum dot occupancy [27,32–34]. The doublet state corresponds to a ground state which is a product state of a free (unscreened) local moment on the quantum dot and a Bardeen-Cooper-Schrieffer (BCS) state in the superconductor, while the singlet state is a precursor state to the Kondo singlet state and consists of an antiferromagnetically aligned state between the QD electron and a Bogoliubov quasiparticle from the superconductor.

In Fig. 3(g), we correlate the lifting of the odd Coulomb valley III with the singlet-doublet ABS QPT. To identify the valley-lifting regime, we plot in a solid line a trace of current along a green dashed line in Fig. 2(a) at $V_{\rm bias} = 1$ mV. When V_S is low, the current is near zero because of Coulomb blockade. As V_S is increased, the dot becomes open and the current starts to increase and finally reaches 4 nA. The inflection point for this crossover occurs at $V_S \approx 110$ mV, the saturation is reached at $V_S \approx 150$ mV. To identify the singlet-doublet transition, we plot the bias voltage of the lowest positive resonance in the center of region III which corresponds to the energy difference between the singlet and the doublet states [$E_s - E_d$, see diagrams in Fig. 3(g)]. We assign positive values of $E_s - E_d$ to looplike resonances (doublet ground state) and negative values to anticrossinglike resonances (singlet ground state). The zero crossing occurs between $V_S \approx 110$ mV and $\approx$200 mV. The data show that the lifting of Coulomb valleys in high-bias transport and the singlet-doublet QPT observed in the subgap region occur roughly within the same range of V_S. In other words, the signatures of odd-parity regimes are erased from transport data at similar dot parameters, both above and below the induced superconducting gap.

These results are reproduced in another device, see supplemental materials [31]. We note that the normal-state tunneling amplitude, a useful scaling parameter, cannot be extracted from these data in a way similar to Ref. [27] because superconductivity cannot be suppressed due to the high critical temperature and field of NbTiN. Also, $V_{\rm bias} = 1$ mV is below the bulk gap of NbTiN (measured to be 2.5 mV), but transport is enabled by the soft gap effect. The soft gap here comes with a finite density of states at the Fermi level. For this reaso, ABS resonances reach zero bias, and there is no need to subtract a bias equivalent to the gap when determining the ABS energies [29].

To numerically analyze the evolution of spectral properties inside and outside the superconducting gap in a simple model setting, we describe the quantum dot using the single-impurity Anderson model,

$$H = \sum_{\sigma} \epsilon\, n_\sigma + U n_\uparrow n_\downarrow + \sum_{k\sigma} (t_k d_\sigma^\dagger c_{k\sigma} + \text{H.c.}) + H_{\rm lead}, \quad (1)$$

where ϵ is the quantum-dot level, $n_\sigma = d_\sigma^\dagger d_\sigma$ is the dot occupancy, U is the electron-electron repulsion parameter, and t_k are the tunneling amplitudes between the dot and the superconducting lead. The coupling between the dot and the lead is quantified by the hybridization strength $\Gamma = \pi |t_k|^2 \rho$, where ρ is the normal-state density of states in the electrode. The lead is described by a BCS Hamiltonian with the gap Δ. In addition, we take into account that the proximitized gap in the quantum dot is soft. The complete information about the lead is contained in the hybridization function in the Nambu formalism. For a BCS Hamiltonian, it takes the form

$$\Delta(z) = \sum_k \frac{|t_k|^2}{z^2 - \xi_k^2 - \Delta^2} \begin{bmatrix} z + \xi_k & \Delta \\ \Delta & z - \xi_k \end{bmatrix}. \quad (2)$$

To describe a hard induced gap, one uses the argument $z = \omega + i0^+$. To model a soft-gap situation, one instead uses $z = \omega + i\delta$ where δ is the finite lifetime of Bogoliubov quasiparticles: This smoothens the BCS coherence peaks as well as produces a finite density of states inside the gap. In this paper, we use $\delta = \Delta/5$. We study the spectral and transport properties of this model using the NRG method [35–37], which consists of discretizing the continuum of states in the leads, transforming the problem into a tight-binding chain form, and iteratively diagonalizing the resulting Hamiltonian. The Wilson chain coefficients that correspond to the generalized BCS hybridization can be computed using the artifactless discretization scheme [38,39] generalized to the matrix case [40]. The spectral function is computed using the density-matrix NRG algorithm. The energy unit is half-bandwidth, $D = 1$. The calculations were performed with the NRG discretization parameter $\Lambda = 2$ by averaging over $N_z = 8$ interleaved discretization grids.

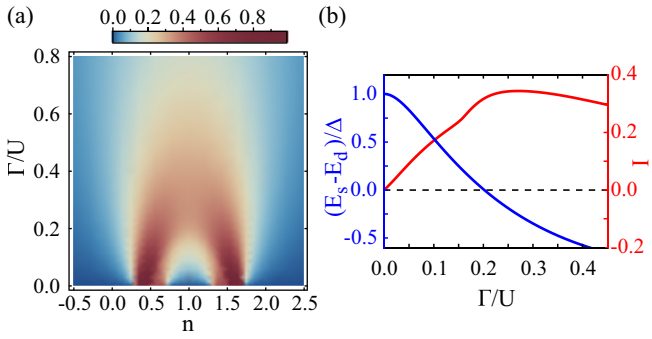

FIG. 4. (a) Simulated finite-bias current (in units of $\pi e t/h$) computed as the integral over the quantum-dot spectral function as a function of the gate voltage (converted to units of charge, n) and the hybridization strength Γ. The electron-electron repulsion parameter $U = 1$. (b) Theoretical singlet-doublet excitation energy splitting (blue line) and finite-bias current (red line) at half-filling, $n = 1$, to be compared with Fig. 3(g). The gap $\Delta = 0.1$, the integration range is from -2Δ to $+2\Delta$.

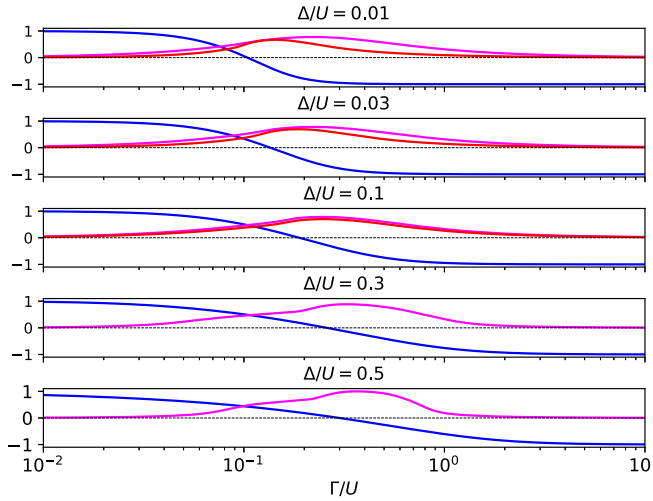

FIG. 5. ABS state energy difference (blue) and the high-bias current for a range of Δ/U. All values are rescaled and plotted without units. The red curves correspond to the integration range $[-U/4 : +U/4]$, the magenta curves correspond to the integration range $[-2\Delta : 2\Delta$ (in this latter case, the values are rescaled for each plot separately).

To approximate the experimental finite-bias transport current within our model, we compute an integral of the quantum dot spectral function in the spirit of the Meir-Wingreen formalism, neglecting any possible nonequilibrium effects, from -2Δ to 2Δ. We first use model parameters $U = 1$, $\Delta = 0.1$, systematically sweeping Γ and ϵ. These results are shown in Fig. 4(a) as a function of the p gate (converted to units of quantum dot charge n) and the contact barrier (expressed as hybridization strength Γ). The superconducting gap terminates the renormalization process and hence plays a similar role as temperature; this is the case even if the gap is somewhat soft. The degree of formation of the Kondo resonance in the impurity spectral function is thus determined by the ratio of T_K/Δ. For $T_K \gg \Delta$ the Kondo resonance is well formed, only the $[-\Delta : \Delta]$ region is truncated. For $T_K \ll \Delta$, there is no Kondo resonance. Because the bias voltage sufficiently exceeds the gap, similar transport processes are relevant as in the normal state. The transport properties are thus also controlled by the ratio of T_K/Δ and the conductance reaches the Kondo plateau value only when T_K exceeds Δ. Indeed, in the weak coupling regime, where $T_K \ll \Delta$, the current is high only at the charge degeneracy points ($n = 1/2$ and $n = 3/2$) due to Coulomb blockade physics. As the coupling increases, so $T_K \sim \Delta$, the current increases in the valley center ($n = 1$), as expected in the emerging Kondo regime; this is the range of $\Gamma/U \approx 0.2$ in Fig. 4(a). In this regime, the $1e$ pattern is no longer observed.

The detailed behavior at $n = 1$ as a function of Γ is shown in Fig. 4(b). We observe that it is qualitatively similar to the rise of current in Fig. 3(g). Some quantitative differences are also noted: In the experiment, the current seems to reach a plateau at large V_S, while in the simulation it decreases at higher Γ due to the breaking down of the Kondo state. The apparent plateau in the experiment for $V_S > 150$ mV in Fig. 3(g) may be due to factors not included in the simplified theoretical model. In Fig. 4(b), we also show the energies of the subgap Andreev bound states, which are extracted directly from the NRG flow diagrams. We find that the singlet-doublet transition occurs at $\Gamma/U \sim 0.2$. For systems with $U \gg \Delta$, as is the case here, this transition is well known to be controlled by the ratio between the Kondo temperature and the superconducting gap and occurs for $T_K \sim \Delta$. This point nearly coincides with the current maximum ($\Gamma/U \sim 0.2$ vs 0.25) and agrees at the qualitative level with the experimental results shown in Fig. 3(b). This agreement is due to the fact that both phenomena occur at the point of maximal competition between the Kondo screening and superconducting pairing, thus they share common origin.

To address the question of generality of this observation that in the model the ABS QPT and the current increase coincide, we perform additional calculations for a wide range of Δ/U at fixed $U = 0.1$. We consider two ways of estimating the current from the spectral function integration: With an integration window $[-2\Delta : 2\Delta]$, as before, and with an integration window $[-U/4 : U/4]$, i.e., a window given by a high bias voltage tied to U rather than Δ, so the high-bias current is more sensitive to charge-fluctuation physics rather than spin physics. The results are shown in Fig. 5. We find that the best correspondence between the zero- crossing of the ABSs and the maximum in high-current bias occurs for moderate Δ/U ratios, but the exact correspondence degrades for very small Δ/U and becomes approximate, especially for the second definition of the bias voltage that is tied to the atomic charge fluctuation scale. In experiments on electrostatically defined quantum dots, U is typically several times Δ, thus in the relevant range the coincidence holds to a very good approximation.

We now discuss experimental data on the singlet-doublet QPT driven by Zeeman splitting, and its relevance to the studies of MBSs. We position the p and s gates in the strong coupled odd regime, where the ground state of the quantum dot is a spin-singlet at zero magnetic field [Figs. 6(a) and 6(b)]. Previous studies have shown that upon

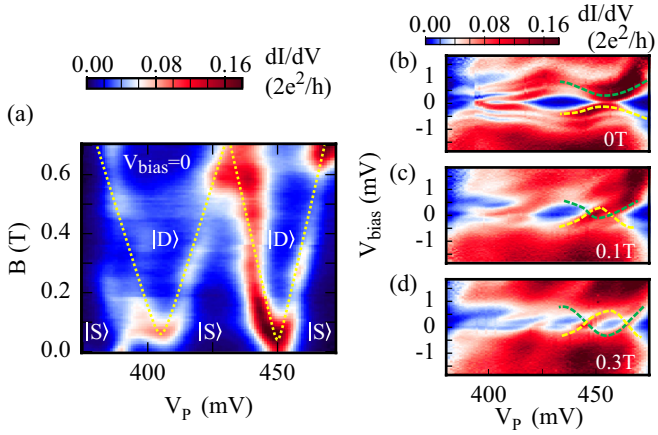

FIG. 6. (a) Zero-bias conductance evolving in magnetic field in the open dot regime ($V_S = 250$ mV in this figure). Ground states of the quantum dot are labeled $|S\rangle$ (singlet) and $|D\rangle$ (doublet). The yellow dashed traces are plots topological superconductivity condition scaled to match the high current contours. (b)–(d) Finite-bias spectroscopy for three values of the magnetic field across the singlet-doublet transition. Yellow and green traces are guides to the eye.

applying magnetic field, a singlet-to-doublet QPT occurs. It is marked by zero-bias peaks that appear when magnetic field shifts the ABS to the middle of the gap [25]. At the same time, zero-bias peaks are intensely studied as signatures of MBSs which accompany a topological QPT.

In Fig. 6(a), we show that the singlet-doublet QPT maps out a similar phase boundary to that expected for topological superconductivity. The data in Fig. 6(a) are obtained at zero bias, thus contours of high current correspond to zero-bias peaks. The guide to the eye has a functional form of a topological phase boundary in an infinite nanowire: $E_Z > \sqrt{\mu^2 + \Delta^2}$, where E_Z is the Zeeman energy, μ is the chemical potential that corresponds to a gate voltage [41,42]. The ground states of the quantum dot are marked with $|S\rangle$ for singlet and $|D\rangle$ for doublet. We observe that the boundary between $|S\rangle$ and $|D\rangle$ regions has a shape similar to the topological phase boundary, most clearly for regime III on the right. Figures 6(b)–6(d) show the magnetic-field-driven singlet-doublet QPT from anticrossinglike to looplike resonances extended in the source-drain bias dimension.

The topological region should correspond to an odd number of one-dimensional subbands crossing the Fermi level, while in this paper we are dealing with odd occupations of a quantum dot. Still, any similarities in data between MBSs and ABSs are important because unintended quantum dots can exist in Majorana devices and those dots can host trivial ABSs. One key difference in appearance between the topological phase of an infinite nanowire and the magnetically driven singlet-doublet QPT is that conductance inside the $|D\rangle$ region is low because the ABS resonances have shifted away from zero bias there, as indicated in Fig. 6(d) where zero-bias peaks are strictly transient. In contrast, MBS resonances should remain at or near zero bias over an area in gate-vs-field map enclosed by the yellow dash-dot trace in Fig. 6(a) [43]. At the same time, ABSs pinned to zero bias have also been reported in quantum dots [25,44–46], and such an ABS can exhibit a similar phase diagram to that found here. Note that here the magnetic field is applied at 30 degrees with respect to the nanowire, so no MBSs are expected because the field has a significant component parallel to the spin-orbit field [47], and ABSs pinning to zero is expected to be reduced as well [48]. We also do not expect MBSs because zero-bias peaks observed here are related to a small quantum dot (smaller than the spin-orbit length). We furthermore remark that the zero-bias conductance is not precisely zero due to resonance broadening and soft gap. Nevertheless, Fig. 6(a) adds to the list of known experimental similarities between ABSs and MBSs [25,29,44–46].

We thank D. Pekker, P. Yu, and A. Zarassi for discussions. S.M.F. is supported by NSF No. DMR-1743972, NSF No. PIRE-1743717, ONR and ARO. R.Ž. acknowledges support from the Slovenian Research Agency (ARRS) under Grants No. P1-0044 and No. J1-7259.

[1] S. Das Sarma, M. Freedman, and C. Nayak, npj Quantum Inf. **1**, 15001 (2015).
[2] M. T. Tuominen, J. M. Hergenrother, T. S. Tighe, and M. Tinkham, Phys. Rev. Lett. **69**, 1997 (1992).
[3] T. M. Eiles, J. M. Martinis, and M. H. Devoret, Phys. Rev. Lett. **70**, 1862 (1993).
[4] P. Lafarge, P. Joyez, D. Esteve, C. Urbina, and M. H. Devoret, Phys. Rev. Lett. **70**, 994 (1993).
[5] S. M. Albrecht, A. P. Higginbotham, M. Madsen, F. Kuemmeth, T. S. Jespersen, J. Nygård, P. Krogstrup, and C. M. Marcus, Nature **531**, 206 (2016).
[6] C. Janvier, L. Tosi, L. Bretheau, Ç. Girit, M. Stern, P. Bertet, P. Joyez, D. Vion, D. Esteve, M. Goffman *et al.*, Science **349**, 1199 (2015).
[7] M. Hays, G. de Lange, K. Serniak, D. J. van Woerkom, D. Bouman, P. Krogstrup, J. Nygård, A. Geresdi, and M. H. Devoret, Phys. Rev. Lett. **121**, 047001 (2018).
[8] T. Matsuura, Prog. Theor. Phys. **57**, 1823 (1977).
[9] K. Satori, H. Shiba, O. Sakai, and Y. Shimizu, J. Phys. Soc. Japan **61**, 3239 (1992).
[10] T. Yoshioka and Y. Ohashi, J. Phys. Soc. Japan **69**, 1812 (2000).
[11] M.-S. Choi, M. Lee, K. Kang, and W. Belzig, Phys. Rev. B **70**, 020502(R) (2004).
[12] A. Oguri and Y. Tanaka, J. Phys. Soc. Jpn. **73**, 2494 (2004).
[13] J. Bauer, A. Oguri, and A. C. Hewson, J. Phys.: Condens. Matter **19**, 486211 (2007).
[14] C. Karrasch, A. Oguri, and V. Meden, Phys. Rev. B **77**, 024517 (2008).
[15] A. Eichler, M. Weiss, S. Oberholzer, C. Schönenberger, A. Levy Yeyati, J. C. Cuevas, and A. Martín-Rodero, Phys. Rev. Lett. **99**, 126602 (2007).
[16] T. Sand-Jespersen, J. Paaske, B. M. Andersen, K. Grove-Rasmussen, H. I. Jørgensen, M. Aagesen, C. B. Sørensen, P. E.

Lindelof, K. Flensberg, and J. Nygård, Phys. Rev. Lett. **99**, 126603 (2007).
[17] C. Buizert, A. Oiwa, K. Shibata, K. Hirakawa, and S. Tarucha, Phys. Rev. Lett. **99**, 136806 (2007).
[18] K. Grove-Rasmussen, H. I. Jørgensen, B. M. Andersen, J. Paaske, T. S. Jespersen, J. Nygård, K. Flensberg, and P. E. Lindelof, Phys. Rev. B **79**, 134518 (2009).
[19] R. S. Deacon, Y. Tanaka, A. Oiwa, R. Sakano, K. Yoshida, K. Shibata, K. Hirakawa, and S. Tarucha, Phys. Rev. Lett. **104**, 076805 (2010).
[20] Y. Kanai, R. S. Deacon, A. Oiwa, K. Yoshida, K. Shibata, K. Hirakawa, and S. Tarucha, Phys. Rev. B **82**, 054512 (2010).
[21] J.-D. Pillet, C. H. L. Quay, P. Morfin, C. Bena, A. Levy Yeyati, and P. Joyez, Nat. Phys. **6**, 965 (2010).
[22] R. Maurand, T. Meng, E. Bonet, S. Florens, L. Marty, and W. Wernsdorfer, Phys. Rev. X **2**, 011009 (2012).
[23] W. Chang, V. E. Manucharyan, T. S. Jespersen, J. Nygård, and C. M. Marcus, Phys. Rev. Lett. **110**, 217005 (2013).
[24] A. Kumar, M. Gaim, D. Steininger, A. Levy Yeyati, A. Martín-Rodero, A. K. Hüttel, and C. Strunk, Phys. Rev. B **89**, 075428 (2014).
[25] E. J. H. Lee, X. Jiang, M. Houzet, R. Aguado, C. M. Lieber, and S. De Franceschi, Nat. Nanotechnol. **9**, 79 (2014).
[26] A. Jellinggaard, K. Grove-Rasmussen, M. H. Madsen, and J. Nygård, Phys. Rev. B **94**, 064520 (2016).
[27] E. J. H. Lee, X. Jiang, R. Žitko, R. Aguado, C. M. Lieber, and S. De Franceschi, Phys. Rev. B **95**, 180502(R) (2017).
[28] Z. Su, A. B. Tacla, M. Hocevar, D. Car, S. R. Plissard, E. P. A. M. Bakkers, A. J. Daley, D. Pekker, and S. M. Frolov, Nat. Commun. **8**, 585 (2017).
[29] Z. Su, A. Zarassi, J.-F. Hsu, P. San-Jose, E. Prada, R. Aguado, E. J. H. Lee, S. Gazibegovic, R. L. M. Op het Veld, D. Car, S. R. Plissard, M. Hocevar, M. Pendharkar, J. S. Lee, J. A. Logan, C. J. Palmstrøm, E. P. A. M. Bakkers, and S. M. Frolov, Phys. Rev. Lett. **121**, 127705 (2018).
[30] G. A. Steele, G. Götz, and L. P. Kouwenhoven, unpublished .
[31] See Supplemental Material at http://link.aps.org/supplemental/10.1103/PhysRevB.101.235315 for additional data and simulations.
[32] A. Martín-Rodero and A. Levy Yeyati, Adv. Phys. **60**, 899 (2011).
[33] D. J. Luitz, F. F. Assaad, T. Novotný, C. Karrasch, and V. Meden, Phys. Rev. Lett. **108**, 227001 (2012).
[34] V. Meden, J. Phys.: Condens. Matter **31**, 163001 (2019).
[35] K. G. Wilson, Rev. Mod. Phys. **47**, 773 (1975).
[36] R. Bulla, T. A. Costi, and T. Pruschke, Rev. Mod. Phys. **80**, 395 (2008).
[37] J.-D. Pillet, P. Joyez, R. Žitko, and M. F. Goffman, Phys. Rev. B **88**, 045101 (2013).
[38] R. Žitko and T. Pruschke, Phys. Rev. B **79**, 085106 (2009).
[39] R. Žitko, Comput. Phys. Commun. **180**, 1271 (2009).
[40] Q.-H. W. Jin-Guo Liu and Da Wang, Phys. Rev. B **93**, 035102 (2016).
[41] R. M. Lutchyn, J. D. Sau, and S. Das Sarma, Phys. Rev. Lett. **105**, 077001 (2010).
[42] Y. Oreg, G. Refael, and F. von Oppen, Phys. Rev. Lett. **105**, 177002 (2010).
[43] J. Chen, P. Yu, J. Stenger, M. Hocevar, D. Car, S. R. Plissard, E. P. Bakkers, T. D. Stanescu, and S. M. Frolov, Sci. Adv. **3**, e1701476 (2017).
[44] M. W. A. De Moor, J. D. Bommer, D. Xu, G. W. Winkler, A. E. Antipov, A. Bargerbos, G. Wang, N. Van Loo, R. L. O. het Veld, S. Gazibegovic *et al.*, New J. Phys. **20**, 103049 (2018).
[45] J. Chen, B. Woods, P. Yu, M. Hocevar, D. Car, S. Plissard, E. Bakkers, T. Stanescu, and S. Frolov, Phys. Rev. Lett. **123**, 107703 (2019).
[46] M. T. Deng, S. Vaitiekenas, E. B. Hansen, J. Danon, M. Leijnse, K. Flensberg, J. Nygård, P. Krogstrup, and C. M. Marcus, Science **354**, 1557 (2016).
[47] C.-H. Lin, J. D. Sau, and S. Das Sarma, Phys. Rev. B **86**, 224511 (2012).
[48] J. D. S. Bommer, H. Zhang, Ö. Gül, B. Nijholt, M. Wimmer, F. N. Rybakov, J. Garaud, D. Rodic, E. Babaev, M. Troyer, D. Car, S. R. Plissard, E. P. A. M. Bakkers, K. Watanabe, T. Taniguchi, and L.P. Kouwenhoven, Phys. Rev. Lett. **122**, 187702 (2019).